Eur. Phys. J. B **23**, 365–372 (2001)

THE EUROPEAN PHYSICAL JOURNAL B

EDP Sciences

Eigenvalues and eigenfunctions of a clover plate

O. Brodier[a], T. Neicu[b], and A. Kudrolli

Department of Physics, Clark University, Worcester, MA 01610, USA

Received 12 February 2001 and Received in final form 17 April 2001

Abstract. We report a numerical study of the flexural modes of a plate using semi-classical analysis developed in the context of quantum systems. We first introduce the Clover billiard as a paradigm for a system inside which rays exhibit stable and chaotic trajectories. The resulting phase space explored by the ray trajectories is illustrated using the Poincare surface of section, and shows that it has both integrable and chaotic regions. Examples of the stable and the unstable periodic orbits in the geometry are presented. We numerically solve the biharmonic equation for the flexural vibrations of the Clover shaped plate with clamped boundary conditions. The first few hundred eigenvalues and the eigenfunctions are obtained using a boundary elements method. The Fourier transform of the eigenvalues show strong peaks which correspond to ray periodic orbits. However, the peaks corresponding to the shortest stable periodic orbits are not stronger than the peaks associated with unstable periodic orbits. We also perform statistics on the obtained eigenvalues and the eigenfunctions. The eigenvalue spacing distribution $P(s)$ shows a strong peak and therefore deviates from both the Poisson and the Wigner distribution of random matrix theory at small spacings because of the C_{4v} symmetry of the Clover geometry. The density distribution of the eigenfunctions is observed to agree with the Porter-Thomas distribution of random matrix theory.

PACS. 05.45.Mt Semiclassical chaos ("quantum chaos") – 46.40.-f Vibrations and mechanical waves

1 Introduction

Sand on vibrating plates (Chladni plates) form interesting nodal patterns. This system is often used to demonstrate the influence of the shape in determining the eigenfunction structure in wave systems. For example, the nodal patterns for square and circular plates show the square and circular symmetry of the plates respectively. The nodal patterns are even more fascinating when a complicated shape is used. Plates shaped as a violin back makes a popular demonstration [1]. The scalar biharmonic equation which is an approximation of the complete vectorial elasto-mechanical equation can be used to describe the lowest eigenfunctions in case of thin plates [2]. Although eigenfunctions for simple integrable shapes such as circular and square plates can be calculated under certain boundary conditions, most (non-integrable) plate shapes such as the violin or the stadium can be obtained by only numerically solving the biharmonic equation.

Because analytical solutions generally do not exist, several techniques have been developed to understand the eigenvalues and eigenfunctions of quantum systems. The two main approaches are (i) semiclassical techniques and (ii) random matrix theory (RMT). Random matrix theory describes the distribution of the eigenvalues for typical systems. For instance, a striking result of this theory is that most systems with strongly chaotic classical limit (and without symmetries) show a universal level distribution [6,7]. Indeed, the spectrum of such a system, provided it is time-reversal invariant, show statistical properities similar to the eigenvalues of a set of random matrices called the Gaussian orthogonal ensemble (GOE). A corollary of this property is that spectrum statistics for a "chaotic" system show level repulsion among neighboring eigenvalues. On the other hand, most systems with integrable classical counterpart show Poisson statistics, where there is no level repulsion.

The semiclassical framework allows us to understand wave properties through the behavior of rays dynamics in the classical limit. Indeed, interesting features of waves in non-integrable shapes can then have satisfactory explanations. For instance the scars phenomenon, which is the concentration of amplitude along short unstable periodic orbits of the corresponding classical system [4]. Earlier work in quantum systems has also shown that the eigenvalues are related to the periodic orbits via trace formulas [5]. The same technique shows that the Fourier transform of the eigenvalues of a wave system is directly related to the length of periodic orbits.

These properties of the eigenvalues and eigenfunctions which depend on the properties of the classical trajectories are expected to hold not only for quantum systems in the semiclassical limit but in any wave system in which the ray limit exhibits chaos. Experiments conducted on a freely vibrating plate shaped as a Sinai-stadium which exhibits ray chaos show complete agreement with GOE

[a] *Present address*: LPTMS, bâtiment 100, 91405 Orsay Cedex, France

[b] e-mail: tneicu@clarku.edu

statistics [8]. Bogomolny and Hugues [9] further argue that the trace formula for the vibration of plates should be similar to that of quantum systems to within a phase factor. They compared the Fourier transform of the eigenvalues of a circular plate and a stadium shaped plate its periodic orbits and found agreement.

However, the ray limits of most waves systems are neither fully chaotic nor integrable and contain islands of integrability. Such systems are often referee to as mixed systems and show a more rich phenomenon compared to systems which are completely chaotic or integrable [10]. Although a universal description has not emerged, these mixed systems show intermediate statistics between completely chaotic and integrable systems. Novel phenomena such as chaos assisted tunneling can occur in this system. The quartic oscillator is often used to study mixed systems [10,11].

In this paper, we introduce the Clover geometry, which is a billiard version of the quartic oscillator with two concave focusing areas, as an example of a mixed system that is suitable for plates. We investigate the ray dynamics by numerically following the trajectories of a ray bouncing inside this geometry. We characterize the phase space using the Poincare surface of section and also give examples of short periodic orbits which may be important in determining the properties of the vibrations of a Clover plate with the same dimensions. We then study the relevance of the ray dynamics on properties of the flexural modes by solving the biharmonic equation with clamped boundary conditions.

A purpose of this work is also to investigate ambivalent results obtained in experiments performed using quartz plates with the Clover shape and free boundary conditions by our group [12]. In this experimental study a Clover shaped quartz plate with free boundary conditions was used. The statistics of the eigenvalues was observed to be intermediate between universal integrable (Poisson) and GOE statistics thus fulfilling the expectation that the presence of integrable regions would lead to deviations from GOE as in the case for quantum systems. However, the strongest peaks in the experimental data does not correspond to the shortest stable periodic orbits. Thus the weak agreement of the peaks with periodic orbits raises many questions which we also investigate in this study of the flexural modes of the Clover with clamped boundary conditions.

2 The classical dynamics in the clover geometry

The Clover geometry consisting of concave and convex arcs is shown in Figure 1. The overall shape is similar to an equipotential curve of the two-dimensional quartic oscillator. Particles or rays launched inside the geometry specularly reflect from the boundaries. The concave boundaries are such that particles launched approximately normal to the boundaries get focused. An example of such a trajectory is shown in Figure 2a. On the other hand the

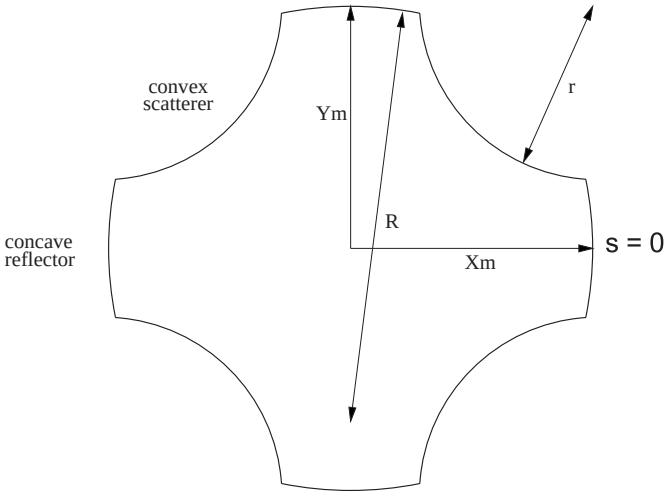

Fig. 1. The Clover geometry is an example of a mixed system containing both chaotic and integrable regions in its classical phase space. ($X_m = Y_m = 1$, $r = 0.7461$, $R = 1.6$.).

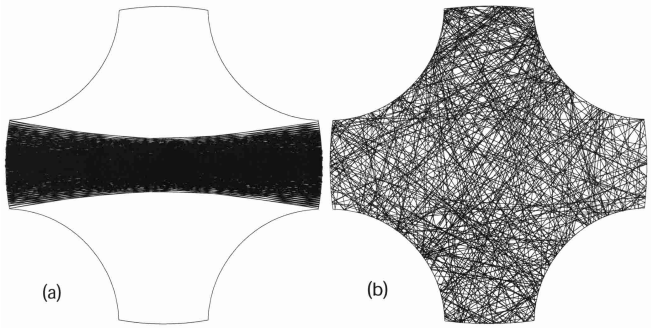

Fig. 2. (a) An example of a ray trajectory inside the Clover geometry shown in Figure 1 which is stable and localized. (b) A trajectory which is unstable.

trajectories that hit the convex side are often chaotic and an example is shown in Figure 2b. The geometry is also highly symmetric and belongs to the C_{4v} point symmetry group. Thus the Clover geometry has the same symmetry as a square.

A convenient method of illustrating the phase space explored by the ray trajectories is using the Poincare surface of section (PSOS). The coordinates on the graph correspond to the distance s along the perimeter where the trajectory hits the boundary and p which is the sine of the angle θ that the ray subtends with the normal to the boundary. Thus s and p define a simplectic (area preserving) map on the Poincare section which associates the $(i+1)$th hit to the i-th hit. The reference point corresponding to $s = 0$ is shown in Figure 1 and $s_{\max}$ is the perimeter of the geometry. It is sufficient to plot the PSOS from $s/s_{\max} = 0$ to $s/s_{\max} = 0.125$ because the PSOS is symmetric about $s/s_{\max} = 0.125$. The full PSOS can be obtained by reflecting the plot about $s/s_{\max} = 0.125$, $s/s_{\max} = 0.25$ and $s/s_{\max} = 0.5$.

The points resulting from launching 500 rays in random directions after 200 bounces is shown in Figure 3 from

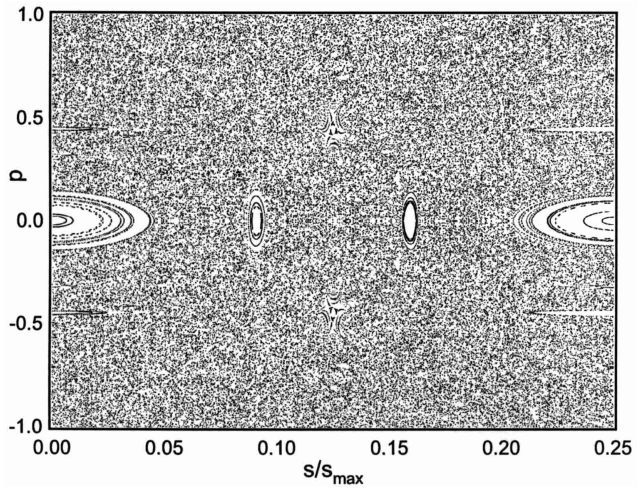

Fig. 3. The Poincaré surface of section (PSOS) shows the chaotic and regular regions. The points are obtained following trajectories with 500 random initial conditions. The PSOS correspond to a Clover geometry with $r = 0.7$ and $R = 1.8$.

$s/s_{\max} = 0$ to $s/s_{\max} = 0.25$. The random speckle points correspond to the chaotic regions and the points along arcs indicate regular regions. Both stable and unstable periodic orbits correspond to a few points that equal the number of bounces at the boundaries. While the points corresponding to unstable orbits are isolated, the stable periodic orbits have a regular region surrounding them. Examples of the shortest stable, unstable and diffractive periodic orbits and their length and stability are listed in Table 1. The regular regions in this case correspond to 6.3% of the total area and therefore the system is essentially chaotic. The fraction and nature of the integrable regions and presence of periodic orbits can be smoothly changed by tuning the various geometric parameters available. The PSOS shown in Figure 3 is fairly similar to that obtained for different values of r and R provided the condition $R > X_m$ and $R > Y_m$ is satisfied. In the limit $R \to \infty$ or if $X_m = Y_m = r$, the geometry is completely chaotic. For a special choice of $r = 0.7461$ and $R = 1.6$, most of the integrable regions correspond to the two shortest stable periodic orbits which are equal in length and are shown in Table 1. The PSOS for these parameters are plotted in Figure 4. Although other stable periodic orbits in Table 1 are still present, they are surrounded by a very small integrable region. Because the PSOS shown in Figure 4 is simpler, we use the corresponding parameters in the simulation of the vibrations of the plate. In the experimental study reported elsewhere [12], the parameters corresponded to the PSOS shown in Figure 3.

3 The wave equation and the boundary conditions in plates

Next we describe the wave equation which we numerically solve for the vibration of thin isotropic plates and its range of validity. In general, the vibration of an acoustic system is very complicated. There are two types of modes in plates: the longitudinal and flexural modes. Because the flexural modes reflect specularly at the boundaries, these modes are ideal to study the effect of periodic orbits compared to the longitudinal modes which undergo mode splitting at the boundaries. The biharmonic equation using the Kirchoff-Love model [2,3] for the amplitude $h(x, y)$ of the flexural modes in the limit of small h is:

$$(\Delta^2 - k^4)h(x, y) = 0, \tag{1}$$

Table 1. The main stable, unstable and diffractive periodic orbits of the Clover geometry and their lengths. The dimensions of the Clover plate are shown in Figure 1.

No	Pattern	Length, L_p (m)	Type	No	Pattern	Length, L_p (m)	Type
1		1.012	diffractive	11		4.295	unstable
2		2.672	unstable	12		4.330	unstable
3		3.060	unstable	13		4.52	diffractive
4		3.20	diffractive	14		4.66	diffractive
5		3.31	diffractive	15		5.67	diffractive
6		3.49	diffractive	16		5.959	stable
7		3.779	unstable	17		7.339	stable
8		4.000	stable	18		7.56	diffractive
9		4.000	stable	19		7.56	diffractive
10		4.013	unstable	20		12.37	stable

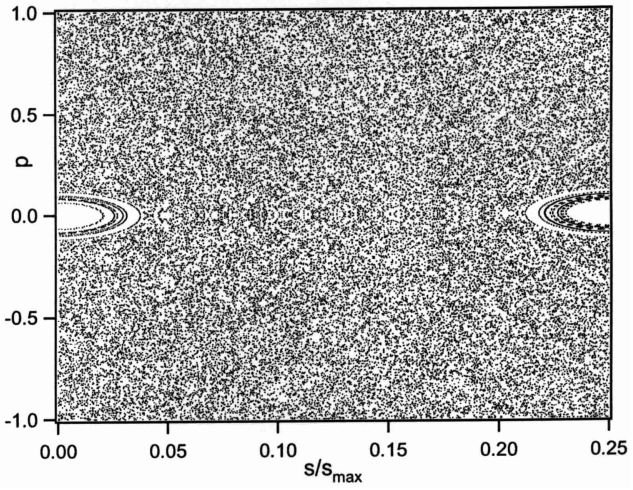

Fig. 4. The Poincaré surface of section shows the chaotic and regular regions. The points are obtained following trajectories with 500 random initial conditions. The PSOS correspond to a Clover geometry with $r = 0.7461$ and $R = 1.6$.

where, Δ is the two-dimensional Laplacian, and k is the wave number.

This equation is obtained using the approximation $kd \ll 1$, where d is the thickness of the plate. In plates with a typical thickness of about 1 mm, this approximation appears to work for the first few hundred modes when compared with experiments [13,12].

The dispersion relation to relate the wave number k to the resonance frequency ω of the plate which is measured experimentally is given by the Kirchoff-Love model as

$$\omega = k^2 \sqrt{\frac{Ed^2}{12(1-\sigma^2)}} \tag{2}$$

where, E is Young's modulus, ρ is the density, and σ is Poisson's ratio. The biharmonic equation generally has two kinds of solutions, propagating modes and non-propagating modes. The non-propagating modes have an exponential form and can exist only near the boundary. A simple derivation of this property of the biharmonic equation can be found in Appendix A. In the case of clamped boundary conditions,

$$h = 0, \text{ and } \frac{\partial h}{\partial n} = 0. \tag{3}$$

The exponential non-propagating modes do not exist for this boundary condition and all the modes are similar to that of a Helmholtz equation for Dirichlet boundary conditions. The only difference arises from the second condition in equation (3).

Experimentally, it is not possible to obtain high quality factors with clamped boundary conditions, and therefore free boundary conditions are used [12]. In case of free boundary conditions, the exponential non-propagating modes can exist but are found to be a small fraction of the modes [9]. To have the simplest possible situation, clamped boundary conditions are used in finding the flexural modes. Thus the possibility of exponential modes giving rise to peaks in the Fourier transform of the experiments [12] can be also tested.

4 Eigenvalues and eigenfunctions of the clover shaped plate

The resonances were obtained using a boundary element method which has been used before to calculate the eigenvalues in quantum billiards [15,16]. However, the Green's function and the Green's formula used for plates is different than for quantum billiards because of the biharmonic equation (Eq. (1)) and the differences in the boundary conditions for plates (see Eq. (3)).

For plates, the boundary element method has been applied in engineering situations for the first few resonances. The method is discussed briefly in Appendix B and is described in detail in reference [14]. To test our numerical implementation of the technique, we have obtained the resonances of a square plate with unit sides and are listed in Table 2. Excellent agreement is observed with the first six eigenvalues reported in reference [14]. Examples of the eigenfunctions of the square plate are shown in the Figure 5.

Table 2. The wave number k_n of the nth flexural mode of a square plate with clamped boundary conditions using the boundary integral equation method (BIE) compares well with the values reported in reference [14]. The units correspond to a plate with unit sides.

k_n	BIE	NASA SP-160	relative error(%)
k_1	5.999	5.999	0
k_2	8.567	8.568	0.01
k_3	10.403	10.405	0.02
k_4	11.471	11.473	0.02
k_5	11.498	11.500	0.02
k_6	12.845	12.851	0.04

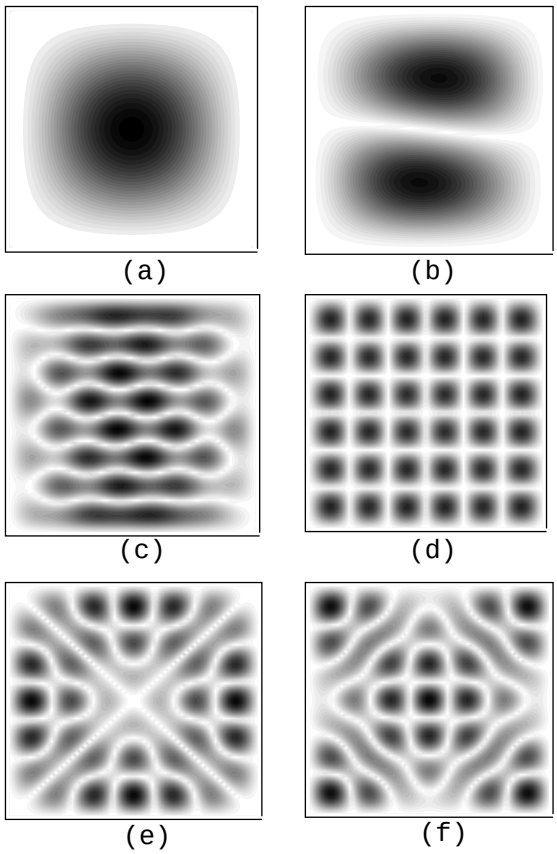

Fig. 5. Examples of numerically obtained eigenfunctions of a square plate. (a) $k = 5.999$, (b) $k = 8.567$, (c) $k = 26.894$, (d) $k = 28.150$, (e) $k = 28.515$, (f) $k = 28.536$. The units correspond to a unit side.

We then obtained the first 281 eigenvalues for the Clover with the dimensions shown in Figure 1 which are below $k = 42.38$. To recognize degenerate modes because of the C_{4v} symmetry of the geometry, we perturbed the

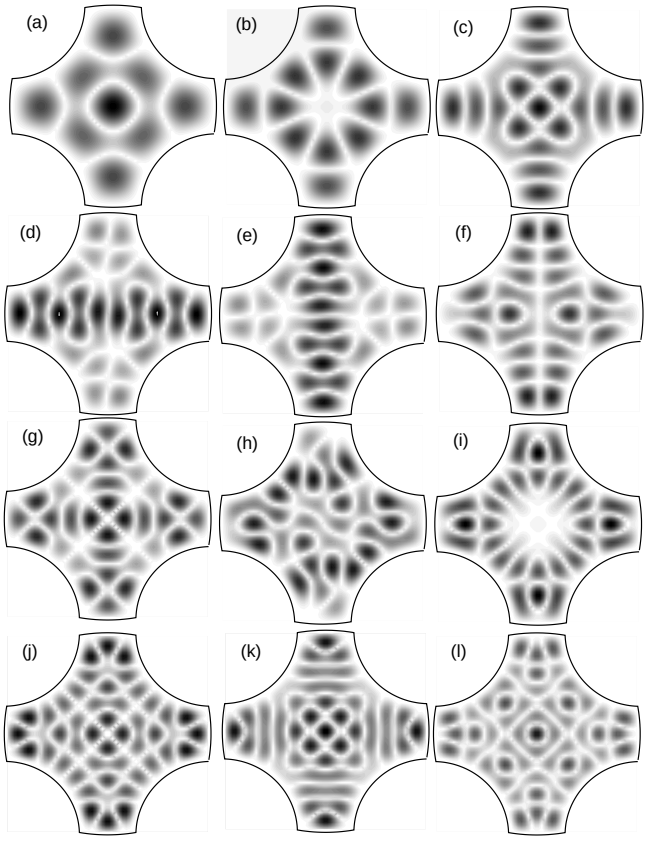

Fig. 6. Examples of numerically obtained eigenfunctions of the clover billiard. (a) $k = 9.982$, (b) $k = 12.239$, (c) $k = 15.656$, (d) and (e) $k = 17.318$, (f) $k = 17.817$, (g) $k = 18.866$, (h) $k = 18.875$, (i) $k = 20.175$, (j) $k = 21.541$, (k) $k = 21.670$, (l)$k = 23.210$. The units correspond to $X_m = 1$.

Clover by changing Y_m by 0.5%. The mean staircase function appropriate for the biharmonic equation [9] is:

$$N(k) = \frac{S}{4\pi} + \beta\frac{L}{4\pi} + c_0, \tag{4}$$

where S and L are the area and the perimeter of the Clover plate respectively, and c_0 is a constant which contains the contributions from the curvature and the corners of the boundary. For the clamped boundary condition, the value of the coefficient is $\beta \approx -1.7627659$ obtained in the semi-classical limit [9]. The mean staircase function for the clamped plate differs from that of the Helmholtz equation with Dirichlet boundary condition where $\beta = -1$. Using the formula, 281 modes are anticipated for $k = 42.40$ which is in excellent agreement with the number of levels obtained in the simulations. Thus we have confidence that the eigenvalues were obtained accurately and no eigenvalues were missed.

Examples of the modes of the Clover are presented in Figure 6. Although most modes appear chaotic, a few of the modes, for example (d) and (e) appear to be localized between the focusing concave sides of the Clover. The examples shown are also degenerate. When the Y_m is increased by 0.5% to split the degeneracy, the mode localized in the longer vertical concave region shifts to a lower eigenvalue, whereas the mode localized in the unperturbed horizontal concave region decreases only very slightly.

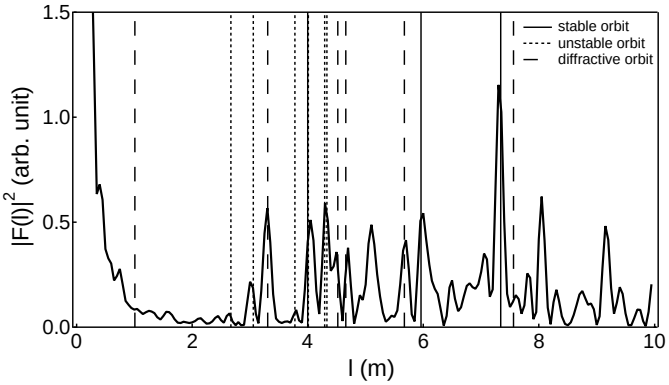

Fig. 7. The Fourier transform $|F(l)|^2$ *versus* l for the Clover plate. The vertical lines correspond to the stable, unstable and diffractive periodic orbits that are plotted in Table 1. The peaks corresponding to the shortest stable orbits are surprisingly not the strongest and a great part of the peaks seem to be associated to diffractive orbits. A few peaks seem not to be explained by any peak, although it is possible that we missed a few periodic orbits since we didn't find a systematic way to find them. On the other hand a few diffractive orbits, which are not represented on the spectrum, correspond to no peak. The results correspond to a Clover plate with the dimensions shown in Figure 1.

5 Fourier transforms

To evaluate the influence of the periodic orbits on the spectral properties of the Clover plate, we calculate the square of the Fourier Transform $|F(l)|^2$ as a function of length l using the formula

$$|F(l)|^2 = n + 2\sum_{i>j,1\le i,j\le n} \cos((k_j - k_i)l). \tag{5}$$

Where n represents the total number of resonances in the spectrum and k_i denotes the wavenumber of the ith eigenvalue. According to theoretical expectations, $|F(l)|^2$ should show strong peaks at values corresponding to the length of the stable and unstable classical periodic orbits, with stronger peaks corresponding to the least unstable orbits.

The $|F(l)|^2$ along with the length corresponding to the shortest periodic orbits is shown in Figure 7. A number of strong peaks are present in $|F(l)|^2$. The position of the peaks are unchanged if the 281 levels are split into two halves and the Fourier transform for each half is calculated. Some of the peaks can be assigned to stable periodic orbits of the Clover geometry (see also Tab. 1), but it is remarkable that most of the peaks seem to correspond to unstable and diffractive periodic orbits. However, there is no obvious correlation between the strength of the peaks and the stability of the corresponding orbits.

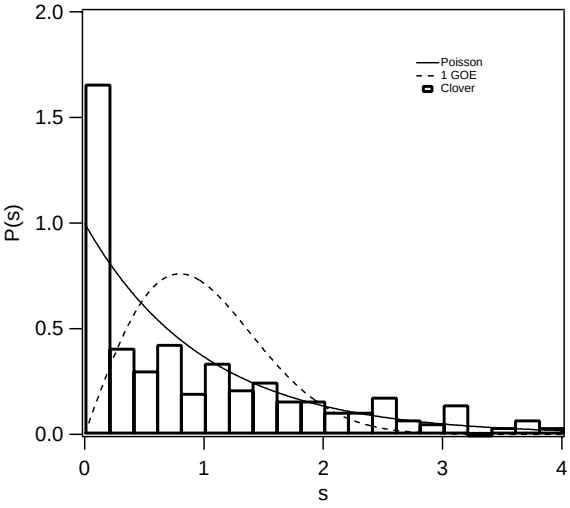

Fig. 8. The spacing statistics $P(s)$ shows level clustering due to the C_{4v} symmetry of the Clover plate ($X_m = Y_m = 1$).

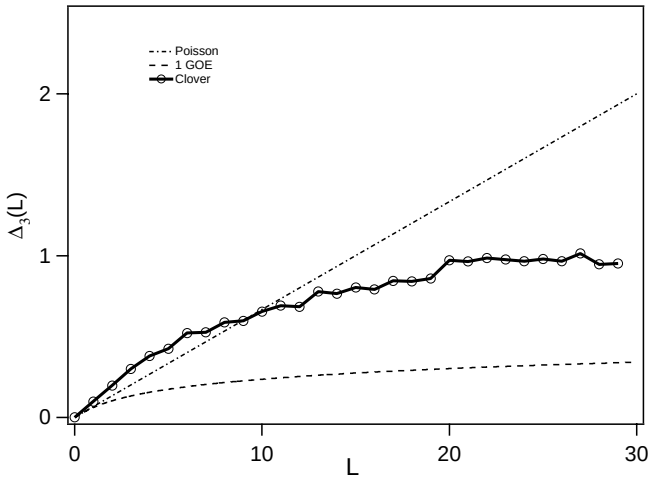

Fig. 9. The spectral rigidity $\Delta_3(L)$ for the Clover plate with C_{4v} symmetry.

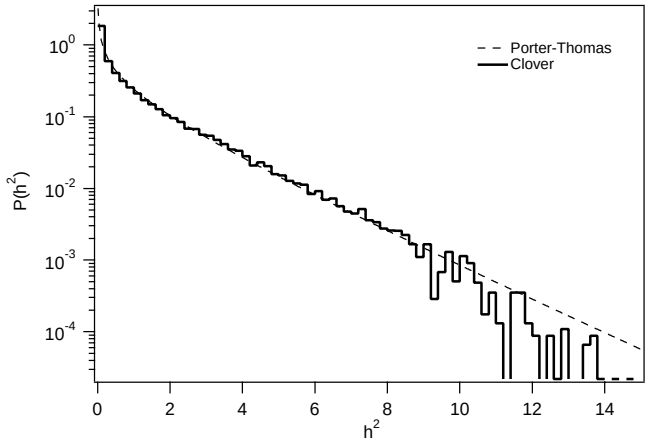

Fig. 10. The $P(h^2)$ *versus* h^2 compared to the Porter-Thomas distribution from Random Matrix theory.

6 The statistics of the eigenvalues and eigenfunctions

After unfolding of the calculated eigenvalues [7], we calculated the distribution of nearest neighbor spacings $P(s)$ where s is the energy difference between the neighboring eigenvalues normalized by the mean energy spacing. As can be seen in the Figure 8, the $P(s)$ deviates from the theoretical predictions corresponding to completely integrable (Poisson statistics) or chaotic systems (Wigner-Dyson statistics) and shows a strong peak in the first bin indicating level clustering due to the high number of degeneracies present in the spectrum.

The degeneracies in the eigenvalues are a direct result of the high spatial symmetry present in the Clover geometry. As mentioned in Section 2, the point symmetry group of the Clover geometry shown in Figure 1 is C_{4v} which has five irreducible representations, one of which is double degenerate [17,10]. The four non degenerate representations each contribute to 1/8th of the number of modes and the double degenerate representation contribute to the remaining half. Therefore, we expect from these symmetry arguments that the fraction of spacings s which contribute to the peak in $P(s)$ to be exactly 25% in the absence of other kind of degeneracies. From our simulations we find that a fraction of 24.5% of the total number of spacings s contribute to the peak. Thus, although the $P(s)$ for a mixed system is expected to show intermediate distribution between Poisson and Wigner ones, in the case of the Clover the distribution appear to have level attraction due to the presence of significant number of degeneracies.

To further quantitatively characterize the eigenvalues, the spectral rigidity $\Delta_3(L)$ is used to study the long range correlations, where L is the length of the interval over which the correlation is calculated. The definition of $\Delta_3(L)$ can be found along with the universal theoretical curves in reference [18]. The $\Delta_3(L)$ curve shown in Figure 9 lies above the Poisson distribution for $1 < L < 9$ due to the high number of degeneracies in the spectra. The $\Delta_3(L)$ for $L > 9$ starts to saturate and lies between the Poisson and GOE distributions.

Although the eigenvalues are sensitive to the spatial symmetry, the eigenfunctions are not sensitive to the symmetries. We used the probability distribution of the squared amplitude of the eigenfunctions $P(h^2)$ to study the properties of the eigenfunctions statistics. The result is shown in Figure 10. The Porter-Thomas distribution is also plotted for comparison:

$$P(h^2) = \frac{1}{\sqrt{2\pi h^2}} \exp\left(-\frac{h^2}{2}\right) \cdot \tag{6}$$

Where h^2 is the squared amplitude of the eigenfunction normalized to unit mean. This distribution can be derived from RMT [20] and describes the case of chaotic systems although deviation may exist in case of significant scarring [19]. In our case the distribution was obtained after averaging eigenfunctions between mode numbers 80 and 281. The $P(h^2)$ for the Clover eigenfunctions are in agreement with the Porter-Thomas formula. Thus the eigenfunctions

for the Clover plate appear to be similar to that of chaotic systems. To quantitatively check this we calculated the Inverse Participation Ratio (IPR), which is defined as:

$$IPR = \langle h^4 \rangle = 1 + c. \tag{7}$$

From the numerical data we obtained $c = 1.996$ which is very close to the value $c = 2.0$ for the Porter-Thomas distribution. Thus the presence of the stable periodic orbits do not appear to significantly alter the $P(h^2)$ at least at the mode numbers investigated.

7 Discussion

We thus find that the properties of the eigenvalues of the biharmonic equation with clamped boundary conditions are consistent with those obtained experimentally using a quartz plate with free boundary conditions [12]. In the experiments, the resonances of a quartz plate with the Clover with C_{4v} symmetry was first obtained between 52 kHz and 352 kHz, and between 800 kHz to 1000 kHz which corresponds with mode numbers 78 to 590, and with 1725 to 2373 respectively. We note that these estimates for the mode number for the higher frequency range was obtained using the three dimensional dispersion relation [12]. The plate was then sanded to reduce the symmetry of the plate to C_{2v} and finally an asymmetric geometry. The Fourier transform of the resonances of the experimental data show peaks corresponding to the main periodic orbit, although a rescaling of the experimental data is required to match the peaks. Thus it appears that the periodic orbits can be observed in both the experiments and the numerical simulations. Although it must be also noted that the strongest peak does not to the shortest stable periodic orbit.

The distributions for $P(s)$ and $\Delta_3(L)$ are also quantitatively similar to that obtained in the experiments for the Clover with C_{4v} symmetry. This indicates that the boundary conditions used, clamped in the simulations presented in the paper, and free in the experiments do not significantly change the statistical properties of the eigenvalues of the Clover plate.

Thus the numerical results along with the supporting experimental results leads us to conclude that direct evidence of periodic orbits in the spectrum are difficult to obtain reliably. It is possible that a better correspondence at higher mode numbers can be made, but it must be noted that in this limit the biharmonic equation ceases to be a good approximation for the complete elasto-mechanical equations that describe the vibration of plates as the wavelength decreases and becomes comparable to thickness of the plate.

We appreciate many fruitful discussions with Steve Tomsovic and Kristian Schaadt. This work was supported by a grant from Research Corporation.

Appendix A

The left hand side of equation (1) can be rewritten as:

$$(\Delta - k^2)(\Delta + k^2)h(x, y) = 0. \tag{A.1}$$

Let h be a solution of this equation. It can be written as:

$$h = \frac{1}{2k^2}(k^2 + \Delta)h + \frac{1}{2k^2}(k^2 - \Delta)h, \tag{A.2}$$

and

$$h = h_1 + h_2. \tag{A.3}$$

Where,

$$(\Delta + k^2)h_1(x, y) = 0, \tag{A.4}$$

and

$$(\Delta - k^2)h_2(x, y) = 0. \tag{A.5}$$

Therefore, $h(x, y)$ can be decomposed into a sum of the solution of the Helmholtz equation $h_1(x, y)$ and an exponential function $h_2(x, y)$.

Appendix B

The Green's function $G(r, r')$ used in solving equation (1) is given by:

$$\begin{aligned} \mathrm{Re}[G(r, r')] &= \frac{1}{8k^2}[N_0(k|r - r'|) + \frac{2}{\pi}K_0(k|r - r'|)], \\ \mathrm{Im}[G(r, r')] &= \frac{1}{8k^2}[-J_0(k|r - r'|)], \end{aligned} \tag{B.1}$$

which is the solution of the equation:

$$(\Delta^2 - k^4)G(X, Y) = -\delta(X - Y). \tag{B.2}$$

The two dimensional problem of integrating the above equation inside the Clover domain is translated to a one dimensional problem at the boundary using the Green's formula. This technique is similar with the usual approach for quantum billiard systems. However, we use a Green's formula appropriate for plates [14]:

$$\int [v(\Delta^2 - k^4)u - u(\Delta^2 - k^4)v]\mathrm{d}A = \int [v(V_n u) - (\partial_n v)(M_t u) + (M_t v)(\partial_n u) - (V_n v)u]\,\mathrm{d}s \tag{B.3}$$

where M_t and V_n are boundary operators and can be found in reference [14]. In this equation we substitute v with Green's function given in equation (B.1), and u with the solution of the plate equation $h(x, y)$ which is to be

determined. The resulting equation using clamped boundary condition (see Eq. (3)) and for a point $X = (x_0, y_0)$ inside the domain can be written as:

$$h(X) = \int_{\partial D} \Big[G(X,l) V_n h(l) - \partial_n G(X,l) M_t h(l) \Big] \mathrm{d}l, \tag{B.4}$$

where n is the normal to the boundary at the point l, and t is a unit vector tangential to the boundary, and

$$\begin{aligned} M_t h(X) &= \Delta h(X) + (1-\nu)\partial_t^2 h(X) \\ V_n h(X) &= \partial_n \Delta h(X) + (1-\nu)\partial_t \partial_n \partial_t h(X). \end{aligned} \tag{B.5}$$

Because we have two boundary conditions, we also need an equation for the first derivative of h. It is sufficient to take the derivative of equation (B.4) in the direction n_X:

$$\begin{aligned} \partial_{n_X} h(X) = \int_{\partial D} \Big[& \partial_{n_X} G(X,l) V_n h(l) \\ & - \partial_{n_X} \partial_n G(X,l) M_t h(l) \Big] \mathrm{d}l. \end{aligned} \tag{B.6}$$

Thus we obtain the value of the solution and its first derivative at a point X inside the domain as an integral function of the value of its derivatives on the boundary. We want equations which only depends on the boundary. Therefore we take the limit of equation (B.4) and equation (B.6) as X goes to the boundary.

In the case of clamped boundary condition, the limit of the integral as X goes to the boundary equals the integral of the limit because the Green's function and its first derivative are not singular. Moreover, the left hand of equation (B.4) and equation (B.6), after taking the limit, is 0. Therefore we get

$$\begin{aligned} 0 &= \int_{\partial D} \Big[G(X,l) V_n h(l) - \partial_n G(X,l) M_t h(l) \Big] \mathrm{d}l \\ 0 &= \int_{\partial D} \Big[\partial_{n_X} G(X,l) V_n h(l) - \partial_{n_X} \partial_n G(X,l) M_t h(l) \Big] \mathrm{d}l \end{aligned} \tag{B.7}$$

where X is now a point of the boundary, and n_X the normal to the boundary at this point.

To evaluate the integrals, the boundary is discretized into N segments. The source points are labeled l_j, and the field point is l_i. These points are now on the boundary and the index i and j run from 1 to N. The unknown variables of these discrete equations are the discrete values of the unknown functions $M_t h(l_i)$ and $V_n h(l_i)$ at the finite set of points l_i:

$$\begin{aligned} M_i &= M_t h(l_i) \\ V_i &= V_n h(l_i). \end{aligned} \tag{B.8}$$

Now we discretize equation (B.7):

$$\begin{aligned} 0 &= \sum_{j=1}^{N} \alpha_1(l_i,l_j) M_j - \alpha_2(l_i,l_j) V_j \\ 0 &= \sum_{j=1}^{N} \beta_1(l_i,l_j) M_j - \beta_2(l_i,l_j) V_j. \end{aligned} \tag{B.9}$$

Where $\alpha_{1,2}$ and $\beta_{1,2}$ are discrete values of the Green's function and its derivatives at points (l_i, l_j) which are known.

The determinant of this system of equations, which is a function of the wave number k, must be equal to zero for a solution to exist:

$$\begin{vmatrix} \alpha_1(l_i,l_j)(k) & \alpha_2(l_i,l_j)(k) \\ \beta_1(l_i,l_j)(k) & \beta_2(l_i,l_j)(k) \end{vmatrix} = 0.$$

This determinant is checked for its minima as a function of k. The k corresponding to the minima are the resonances of the plate.

The eigenfunctions corresponding to a resonance can be calculated by extending the method further. By solving the system of equations (Eq. (B.9)) for a given resonance k, we get a set of discrete values of the derivatives of the solution at the boundary $M_t h(l_i)$ and $V_n h(l_i)$. By introducing these values in the Green's (B.4) formula we can obtain the solution $h(x, y)$ everywhere inside the domain.

References

1. *Demonstrations in wave motion*, CENCO Physics Catalogue (2000).
2. L.D. Landau, E.M. Lifshitz, *Theory of Elasticity* (Addison-Wesley, Reading, 1959).
3. K.F. Graff, *Wave Motion in Elastic Solids* (Dover Publications, New York, 1975).
4. E.J. Heller, Phys. Rev. Lett. **53**, 1515 (1984).
5. M. Gutzwiller, *Chaos in Classical and Quantum Mechanics* (Springer-Verlag, 1990).
6. O. Bohigas, M.J. Giannoni, C. Schmit, Phys. Rev. Lett. **52**, 1 (1984).
7. M.L. Mehta, *Random Matrices*, 2nd edn. (Academic, New York, 1990).
8. K. Schaadt, A. Kudrolli, Phys. Rev. E **60**, R3479 (1999).
9. E. Bogomolny, E. Hugues, Phys. Rev. E **57**, 5404 (1998).
10. O. Bohigas, S. Tomsovic, D. Ullmo, Phys. Rep. **223**, 43 (1993).
11. S. Tomsovic, D. Ullmo, Phys. Rev. E **50**, 145 (1994).
12. T. Neicu, K. Schaadt, A. Kudrolli, Phys. Rev. E **63**, 026206 (2001).
13. K. Schaadt, M. Sc. Thesis, Niels Bohr Institute (1997).
14. M. Kitahara, *Boundary Integral Equation Methods in Eigenvalue Problems of Elastodynamics and Thin Plates* (Elsevier, 1985).
15. M.V. Berry, Ann. Phys. **131** 163 (1981).
16. P. Gaspard, S.A. Rice, J. Chem. Phys. **90**, 2255 (1990).
17. M. Tinkham, *Group Theory and Quantum Mechanics*, (McGraw-Hill, 1964).
18. M.V. Berry, Proc. R. Soc. London A **400**, 229 (1985).
19. L. Kaplan, E.J. Heller, Phys. Rev. E **59**, 6609 (1999).
20. F. Haake, *Quantum Signatures of Chaos* (Springer-Verlag, Berlin, 1991).